Electrochemistry of Catalytically Graphitized Ball Milled Carbon in Li Batteries

Electrochemistry of Catalytically Graphitized Ball Milled Carbon in Li Batteries

Xiuyun Zhao,[a,b,c] Yuan Yao,[a,b] A. E. George,[a,b] R. A. Dunlap,[a,b,d] and M. N. Obrovac[a,b,c,*,z]

[a]*Department of Physics and Atmospheric Science, Dalhousie University, Halifax, Nova Scotia B3H 4R2, Canada*
[b]*Institute for Research in Materials, Dalhousie University, Halifax, Nova Scotia B3H 4R2, Canada*
[c]*Department of Chemistry, Dalhousie University, Halifax, Nova Scotia B3H 4R2, Canada*
[d]*College of Sustainability, Dalhousie University, Halifax, Nova Scotia B3H 4R2, Canada*

High carbon Fe-C composites with starting concentrations of 10, 20, 30, and 40 wt% Fe (2.3 - 12.5 atomic % Fe) were prepared by ball milling followed by annealing. Increasing the Fe concentration and annealing temperature resulted in catalytic graphitization of the carbon. Mössbauer spectroscopy analysis indicated that Fe concentration and annealing temperature had significant effects on the Fe magnetic hyperfine field, quadrupole splitting, and the formation of γ-Fe. When used as electrodes in Li cells, the electrochemistry of ball milled Fe-C powders annealed at low temperatures resembled that of amorphous carbon. Fe-C with 40 wt% Fe annealed at 2000°C had electrochemical characteristics of a pristine graphite electrode with good cycling performance. These results demonstrate that lithium battery negative electrodes with good cycling performance can be produced from catalytically prepared graphite.

Manuscript submitted January 4, 2016; revised manuscript received February 15, 2016. Published March 3, 2016.

Many structural types of carbon have been extensively studied for use as negative electrodes for Li-ion batteries. Dahn et al. summarized the relationship between capacity and heat-treatment temperature (HTT) of hard and soft carbons as shown in Figure 1.[1] Inexpensive hard carbons with high gravimetric capacities may be made at low HTT (~1100°C), however their volumetric capacity is low. Dense, artificial graphites used in commercial cells, such as mesocarbon microbeads (MCMB), are created by carbonizing soft carbon precursors, such as petroleum pitch, to high HTTs (>2800°C).[2] Such graphites combine high volumetric and gravimetric capacity, low average voltage, and excellent rate performance. However, the high temperature process adds significantly to their cost. Natural graphites have been used more extensively in Li-ion batteries in recent years because of their low cost.[2,3] However, natural graphites can suffer from rate performance issues due to their highly oriented nature, which can cause impeded Li-diffusion in densified electrodes.

The processing temperature of artificial graphites, and hence their cost, can be lowered considerably via the addition of a metal catalyst.[4,5] Catalysts can also induce the graphitization of "non-graphitizable" hard carbon precursors.[5] Group 8–10 metals, such as Fe, Co, and Ni, which have the ability to dissolve carbon, have been shown to be particularly good graphitization catalysts.[4,5] For instance, Baraniecki et al. found that inclusions of 10–40 wt% iron particles in carbon mixtures of calcined petroleum coke, binder pitch and carbon black, led to extensive graphitization after annealing for over 40 hours at temperatures as low as 1600°C.[6]

Considering these results, catalytic graphitization may provide a low cost route to high performance graphites for negative electrodes in Li-ion batteries. Recently, we have shown that graphite synthesized at 1200°C from hard carbon and an iron catalyst can have the same properties artificial graphites made at high temeperatures[7] Apart from this, to our knowledge the electrochemistry of fully graphitized catalytically derived carbons has not been reported. Instead, there have been a number of studies recently on the electrochemistry of carbons prepared with transition metal particles at low heat-treatment temperatures (HTT ≤ 1000°C). Such carbons have voltage curves typical of disordered carbons,[8–10] however the presence of the metal particles results in significantly increased reversible carbon capacity. Skowronski et al. graphitized hard carbon with an iron catalyst at 1000°C to form a graphite with turbostratic disorder with superior rate performance to flake graphite.[11] These encouraging results prompted us to study the electrochemistry of fully graphitized catalytically derived carbons.

Ball milling and sputtering have proved to be useful methods for preparing high carbon Fe-C materials.[12–15] Tanaka et al.[12] prepared $Fe_{1-x}C_x$ (x = 0.17–0.90) by mechanical alloying and found evidence on the basis of Mössbauer effect studies for the formation of a paramagnetic phase with x = 0.80–0.90. Wang et al.[13] obtained $Fe_{1-x}C_x$ (x = 0.80) powders by ball milling and observed that a powder milled for 45 h contained α-Fe and the austenite γ-Fe phase, while a powder milled for 140 h contained a disordered Fe_3C phase. In our recent work, carbon-rich $Fe_{1-x}C_x$ ($0.35 \leq x \leq 0.97$) films were sputtered and their structural and electrochemical properties were investigated by X-ray diffraction (XRD), Mössbauer effect spectroscopy and electrochemical techniques.[14,15] The presence of Fe was found to significantly increase the reversible capacity per mass of carbon over that of a pure carbon electrode.[15] To the best of our knowledge, there have not been detailed Mössbauer effect or electrochemical studies of high carbon $Fe_{1-x}C_x$ (x > 0.90) materials.

Ball milled carbons have been studied as negative electrodes in the past,[16,17] and the previously reported capacities of ball milled

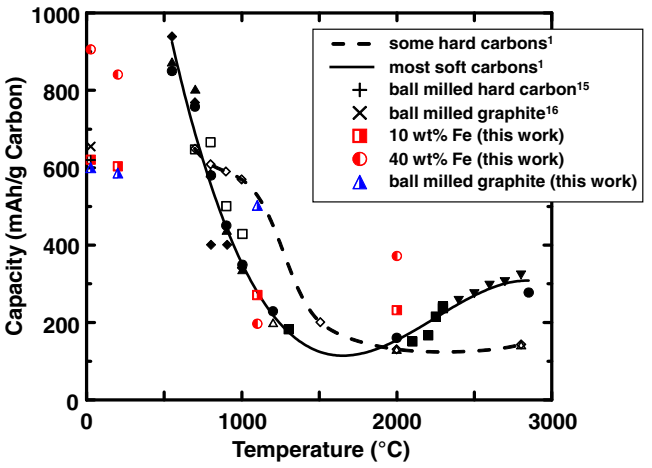

Figure 1. Plot of reversible capacity for lithium versus heat-treatment temperature of hard and soft carbons made with no catalyst; adapted with permission from Reference 1. Overlaid on this plot are data from ball milled carbon [Reference 15], ball milled graphite [Reference 16] and the performance characteristics of catalytically derived carbons from the present study.

*Electrochemical Society Member.
[z]E-mail: mnobrovac@dal.ca

hard carbons are included in Figure 1. Such carbons are not dense and are highly reactive toward air. Like hydrogen containing carbons, their voltage curves have substantial hysteresis, although their hydrogen content is low.[16,17] Xing et al. suggested that such carbons can contain edge carbons terminated by dangling bonds that react with lithium to produce similar voltage curve features as hydrogen containing carbons.[17] Annealing ball milled carbons could potentially eliminate free radical carbon. To our knowledge, annealed ball milled carbons have not been previously studied as negative electrodes in lithium batteries.

In the present work, we have prepared disordered and catalytically graphitized carbons from ball milled Fe-C powders with 10 - 40 wt% Fe ($0.87 < x < 0.98$ in $Fe_{1-x}C_x$) that were subsequently annealed at 200°C - 2000°C. The structures of the Fe-C samples were studied by XRD and room temperature ^{57}Fe Mössbauer effect spectroscopy. The electrochemistry of the Fe-C materials was then investigated by incorporating them in electrodes and evaluating their performance in lithium batteries.

Experimental

Sample preparation.—Starting materials used for ball-milled Fe-C were graphite (MAG-E, Hitachi) and Fe powder (Alfa Aesar, 99.9% pure, <10 μm). Ball milling was carried out using a SPEX mill (Model 8000-D, SpexCertiprep, Metuchen, NJ). 2.26 g of precursor powder along with 115 g WC balls (3/16 inch in diameter) were loaded inside a 65 mL hardened steel vial under Ar. Ball milling was carried out for 2 hours. For samples annealed at 200°C and 1100°C, the milled powder was transferred into a combustion boat in an Ar glove box and annealed in a tube furnace for 3 h under flowing argon. All steps were performed in Ar in order to avoid the reaction of the freshly ground powders with oxygen in the air.[17]

For samples heated to higher temperatures, an RF induction furnace was used. This furnace had no means of transferring samples without air exposure. Therefore, milling vials containing samples for induction heating were first cooled completely to room temperature. The milling vial was then opened slightly, to very slowly introduce the sample to air. After that, the powders were transferred to a graphite crucible and annealed at 2000°C using an RF induction furnace vacuum chamber (Philips PH1100) powered by a 10 kW RF power supply (Pillar Industries MK-20) operating at approximately 350 kHz. The heating chamber was evacuated to a pressure of less than 10^{-4} Torr and backfilled with Ar. The temperature was monitored with a 2-color infrared optical pyrometer (IRCON MR-OR05-24C) through an optical viewport in the vacuum chamber.

To evaluate the carbon content of the 40 wt% Fe sample annealed at 2000°C, thermogravimetric analysis (TGA) was carried out on a TG 209 F3 thermo-microbalance (NETZSCH, Germany) between 25°C and 900°C with a heating rate of 5°C/min in flowing air atmosphere.

X-Ray diffraction measurements.—XRD patterns were collected using a Rigaku Ultima IV diffractometer with a CuK_α radiation source ($\lambda = 1.54$ Å), a diffracted-beam graphite monochromator and a scintillation detector. The goniometer radius was 285 mm, the incident slit width was 10 mm, the receiving slit width was 0.3 mm, and the beam width was 7 mm. An accelerating voltage of 45 kV and a filament current of 40 mA were used to generate X-rays. Measurements were taken from 20 to 60 or 10 to 120 degrees in 2θ, at intervals of 0.05 degrees. Step times of 3 s per interval were employed for most of samples and a fixed time of 8 s was employed for the sample used for structure refinement. All XRD patterns were corrected for the Lorentz-polarization factor (LPF) and the square of the carbon atom scattering factor, to remove distortion at low angles, as described by Dahn et al.[18]

Mössbauer effect spectroscopy measurements.—Room temperature ^{57}Fe Mössbauer effect spectra were collected using a resonant gamma-ray spectrometer (Model W302 from SEE Co.) equipped with a $Rh^{57}Co$ source. The velocity scale was calibrated relative to room temperature α-Fe. Lorentzian site analysis was performed using RECOIL software.[19] A Phenom G2-pro Scanning Electron Microscope (SEM, Nanoscience, AZ) was used to observe the morphology of the samples. The density was measured using a Micromeritics AccuPyc II 1340 Pycnometer.

Electrochemical measurements.—All electrodes were prepared under an Ar atmosphere. Electrode slurries containing 90 wt% active powder, 2 wt% Super-P carbon black (MMM Carbon, Belgium) and 8 wt% polyvinylidenedifluoride (KYNAR) binder in 1-Methyl-2-pyrrolidinone (Sigma-Aldrich, 99.5%) were mixed using a Kurabo Mazerustar planetary mixer/deaerator for two cycles (600 s total). A thin layer of slurry was coated on Cu foil using a Teflon coating bar with a 0.004 inch gap. The electrodes were dried in vacuum at 120°C overnight before use. The electrolyte was 1 M $LiPF_6$ dissolved in ethylene carbonate / diethyl carbonate / monofluoroethylene carbonate [30/60/10, v/v/v]. 2325 coin-type cells with two Celgard 2300 separators and a lithium foil common counter / reference electrode were assembled in an argon-filled glove box using the electrodes described above.

For all cells, the same electrochemical testing protocol was used. The theoretical capacities of all samples were calculated assuming that only carbon is active with a theoretical capacity of 372 mAh/g and that Fe is inactive to lithium. Cells were cycled with a Maccor Series 4000 Automated Test System at a C/10 rate and trickled discharged to C/40 in the first cycle and a C/5 rate and trickled discharged to C/20 for all subsequent cycles, in a voltage range of 0.005-2.0 V.

Results and Discussion

Structural characterization by XRD.—The LFP corrected XRD patterns of the as-milled, 200°C and 1100°C annealed Fe-C samples as a function of Fe concentration are shown in Figure 2. Also shown are the known peak positions of graphite (JCPDS 96-901-2231), Fe (JCPDS 00-006-0696), and WC (JCPDS 00-051-0939).[20] In Figure 2, the main peak at about 26° can be attributed to the C(002) refection for all samples. The 44° peak is corresponding to C(101) reflection for carbon samples. For the Fe-C samples, this peak can be contributed from both carbon and Fe or some iron carbides. As well, the peaks at about 36° and 47° are identified as tungsten carbide (contamination from the tungsten carbide balls used during ball milling). The XRD patterns for the samples annealed at 200°C are almost identical to those of the as-milled Fe-C samples. Samples of all compositions annealed at 1100°C show considerable sharpening of both the C(002) peak and the Fe(110) peak compared to samples annealed at 200°C, indicating that the higher temperature improves the crystallinity of carbon and iron. At 1100°C, as the C(002) peak becomes especially narrowed as the Fe content is increased, indicating an increased level of graphitization, as will be discussed below. In addition to the identified peaks from Fe and C, some small peaks near 43° can be observed, however these peaks could not be identified.

Figures 3a and 3b show the XRD patterns of ball-milled Fe-C samples with 10 wt% and 40 wt% Fe annealed in Ar at 2000°C, respectively. These samples have much more defined C(002) peaks compared to those shown in Figure 2. The 10 wt% Fe sample is typical of a turbostratically disordered graphite.[21] However, the pattern has two C(002) peaks, a large broad peak and the other a small sharp peak, presumably from a disordered carbon phase and a well crystallized graphite phase,[4] respectively. The 40 wt% Fe sample has a sharp C(002) peak characteristic of well graphitized carbon.

In order to quantify the changes that occurred during annealing, C(002) peaks were fit with pseudo-Voigt peak profiles and a quadratic background function using a least squares fitting routine. The Scherrer equation was used to determine the stacking height (L_c) of the graphite crystallites from the peak widths. The lateral size (L_a) was not calculated because the peaks of carbon and Fe at about 44° are almost coincidental, as shown in Figure 2, making them difficult to disambiguate. Table I lists the values of L_c as determined from the

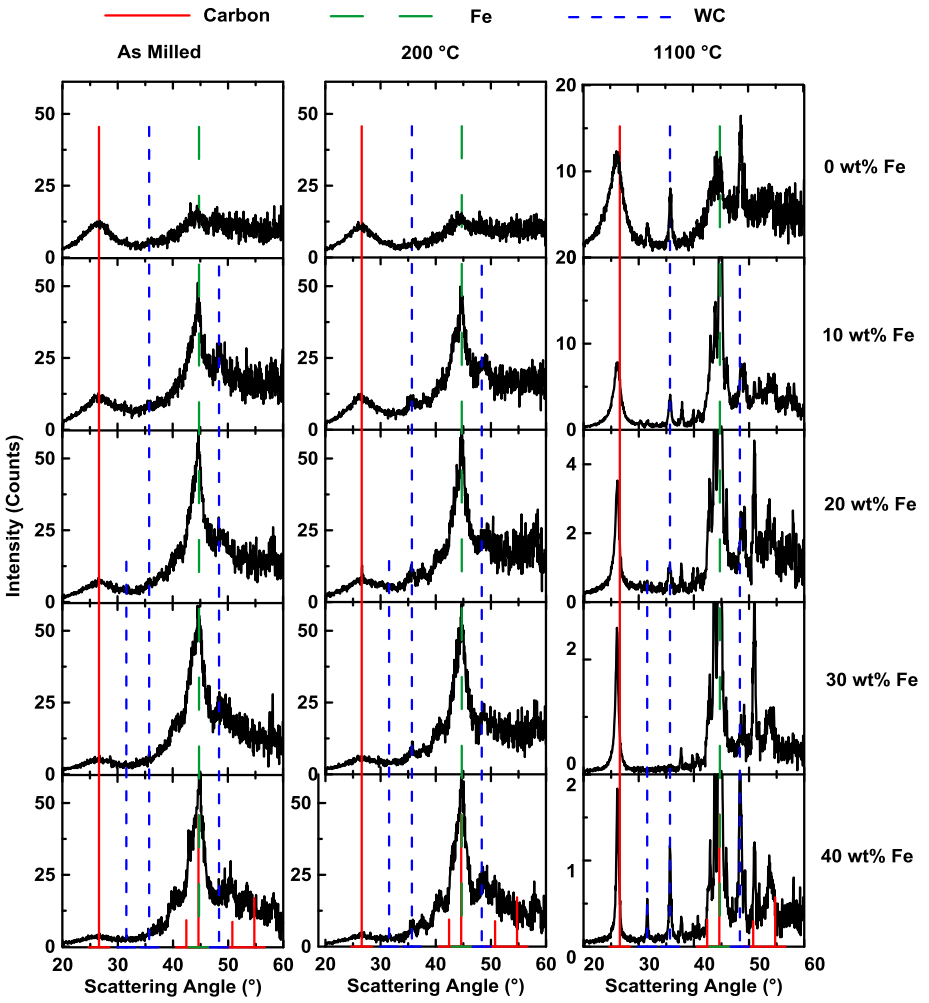

Figure 2. XRD patterns of Fe-C powders before and after annealing at 200°C and 1100°C, respectively (Fe content in the starting materials: 0–40 wt% as indicated on the right side of the figure).

Table I. Structural parameters extracted from the curve fitting of XRD patterns for the Fe-C powders milled for 2 hours as-milled and after annealing at 200°C, 1100°C, and 2000°C. Typical uncertainties in fitted parameters are ±0.2° for 2θ, ±0.005 nm for d(002), ±0.005° for FWHM, and ±0.1 nm for L_c.

Sample	2θ (002) (degrees)	d (002) (nm)	FWHM (002) (degrees)	L_c (nm)
As milled, 0 wt%	26.4	0.338	5.881	1.4
200°C , 0 wt%	26.3	0.339	5.926	1.4
1100°C, 0 wt%	26.0	0.342	2.943	2.7
As milled, 10 wt%	26.5	0.336	6.265	1.3
200°C , 10 wt%	26.4	0.338	6.374	1.3
1100°C, 10 wt%	26.0	0.342	1.433	5.6
2000°C, 10 wt%	25.8 (92.5%)	0.345	1.214	6.6
	26.5 (7.5%)	0.336	0.142	56.9
As milled, 20 wt%	26.4	0.337	6.664	1.2
200°C , 20 wt%	26.4	0.337	6.580	1.2
1100°C, 20 wt%	26.1	0.342	1.071	7.5
As milled, 30 wt%	26.5	0.336	7.171	1.1
200°C , 30 wt%	26.5	0.336	7.181	1.1
1100°C, 30 wt%	26.1	0.341	0.593	13.6
As milled, 40 wt%	26.4	0.337	7.916	1.0
200°C , 40 wt%	26.4	0.337	7.926	1.0
1100°C, 40 wt%	26.2	0.340	0.477	16.9
2000°C, 40 wt%	26.2 (15.9%)	0.340	0.364	22.1
	26.5 (84.1%)	0.336	0.141	57.3

C(002) peak for the as-milled Fe-C samples. The L_c values of the as-milled Fe-C powders are about 1 nm, indicating a highly disordered carbon structure. The peak parameters of the samples annealed at 200°C are very similar to those of the as-milled samples, indicating the stability of ball-milled Fe-C powders at this temperature. For the samples annealed at 1100°C, the value of L_c increases from 2.7 nm to 16.9 nm with increasing of Fe concentration from 0 wt% to 40 wt%. For the Fe-C sample with 10 wt% Fe annealed at 2000°C, the value of L_c for the broad major C(002) peak is 6.6 nm, however, a much sharper minor peak with a L_c of 56.9 nm also appears that is characteristic of graphite. For the Fe-C sample with 40 wt% Fe annealed at 2000°C, the XRD pattern comprises a very sharp major C(002) peak characteristic of graphite and the L_c is 57.3 nm with a very minor C(002) peak having a smaller L_c value of 22.1 nm. The relative area ratio of the broad peak and sharp peak varies from 92.5/7.5 to 15.9/84.1 with increasing Fe from 10 wt% to 40 wt%, indicating that 40 wt% Fe content has caused nearly complete graphitization of ball milled carbon at this temperature.

To further evaluate the graphitization degree of the Fe-C sample with 40 wt% Fe annealed at 2000°C, Fe or iron carbides were removed from this powder by HCl solution. The resulting carbon was identified by XRD and the structure refinement program (CARBONXS) developed by Hang and Reimers et al.[21] was used to measure the structure parameters of this carbon. Figures 3c shows the measured, calculated, and difference profiles (using the two-layer model).[21] Small iron peaks still can be observed from the XRD patterns, however, the calculated model fits the XRD patterns of carbon powders very well, when the iron peaks are neglected. The fitted d(002) spacing is 3.3551(6) Å, the

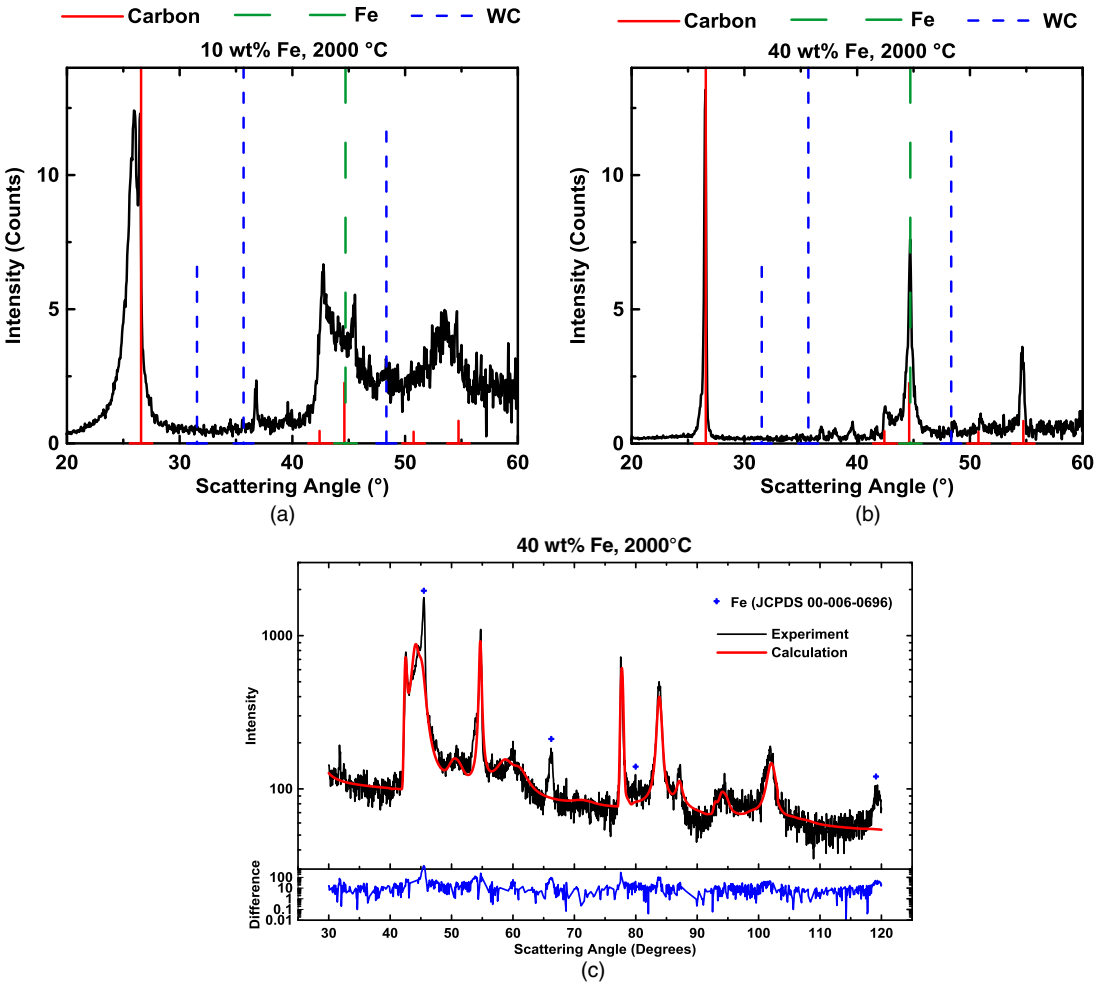

Figure 3. XRD patterns of Fe-C powder with (a) 10 wt% Fe and (b) 40 wt% Fe in starting materials, after annealing at 2000°C. (c) Measured, calculated and difference XRD profiles for the carbon obtained from the Fe-C powder with 40 wt% Fe after annealing at 2000°C.

probability of random stacking (P_r) is 0.136(8), and the probability of 3R stacking (P_t) is 0.139(6). The value of P_r is larger than that of commercial graphite from Johnson Matthey Inc (JMI) ($P_r = 0.05$), and is similar to that of annealed MCMB at 2800°C ($P_r = 0.10$), as reported in Ref. 22. This indicates that the carbon obtained for the present work at 2000°C shows a high degree of graphitization, even surpassing that of some commercial graphites annealed at much higher temperatures, and may have excellent potential for application as anode material of lithium ion batteries.

Mössbauer effect spectroscopy characterization.—Mössbauer effect spectroscopy is more sensitive to the local structure of Fe-containing phases than XRD. Figures 4a–4c show the room temperature Mössbauer effect spectra of ball milled Fe-C samples as a function of Fe concentration and annealing temperature. Spectra were fit to combinations of Lorentzian singlets, doublets and sextets as appropriate for each spectrum. Doublet components were constrained to be symmetric. The relative areas of the six peaks for sextet components have been fixed to 3:2:1:1:2:3 as appropriate for non-textured powder samples. Both the value of the ratio (w1/w3) of the half-width at half maxima (HWHM) of peak 1 and peak 3 and the value of the ratio (w2/w3) of the HWHM of peak 2 and peak 3 were allowed to vary during fitting, however, their values remained close to 1. The results from the fitting of these spectra are listed in Table II. Here, δ is the center shift, Δ is the quadrupole splitting, H is the hyperfine magnetic field, Γ is the HWFM, and A is the relative area of the subspectrum.

For the Fe-C samples both before and after annealing at 200°C, as shown in Figure 4a, all spectra consisted of two quadrupole split doublets and three magnetically split sextets. As listed in Table II, the center shifts and quadrupole splittings for the two doublets are very similar for all samples before and after annealing at 200°C. The values of the three hyperfine fields are around 33.0 T, 20.0 T, and 11.5 T. However, it can be observed that the intensity of the sextets increases while the intensity of the doublets decreases with increasing of Fe content based on the relative areas of different components. The sextet with a hyperfine field of about 33.0 T with a center shift of near zero indicates the presence of the α-Fe phase, and the lower magnetic hyperfine fields of about 20.0 T is consistent with the presence of the Fe_3C phase. These values are in good agreement with those reported for α-Fe and Fe_3C in ball-milled Fe-C materials with both low[23] and high[12] carbon content. The hyperfine field of about 11.5 T cannot be assigned to a specific Fe-C phase. However, this lower hyperfine field suggests the presence of Fe sites with fewer Fe and more C near neighbors than in the Fe_3C phase. The two doublet sites correspond to paramagnetic phases where the site with the more positive center shift corresponds to Fe atoms which have more carbon neighbors; while the site with a less positive center shift corresponds to Fe atoms that have fewer carbon neighbors. Moreover, the relative concentration of paramagnetic phases decreases while the relative concentration of ferromagnetic phases increases with increasing of Fe content.

In summary, based on the fitted Mössbauer parameters in Table II, the as-milled and 200°C samples comprise iron in the form of α-Fe, paramagnetic Fe, Fe_3C and unidentified Fe-rich Fe-C phases.

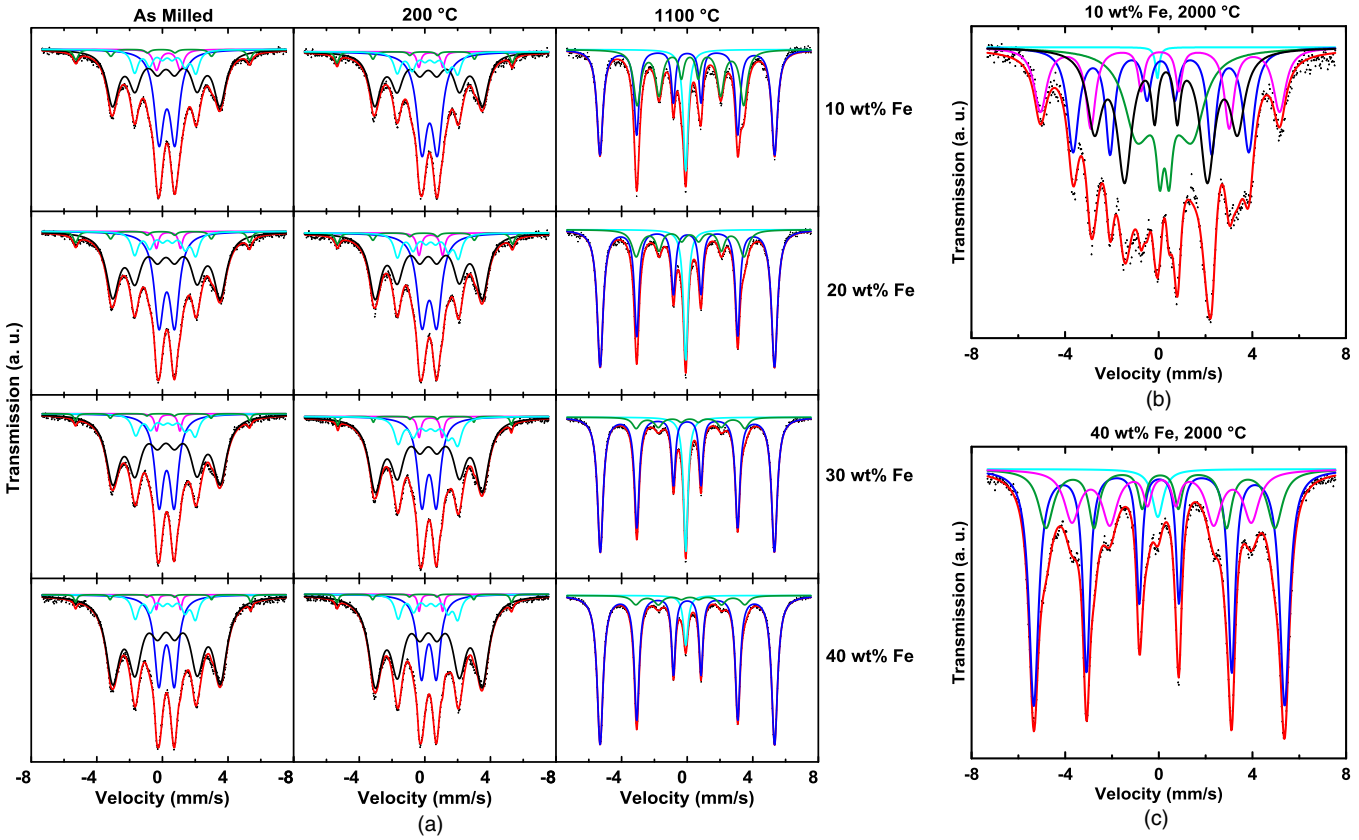

Figure 4. (a) Room temperature ^{57}Fe Mössbauer spectra of Fe-C powders before and after annealing at 200°C and 1100°C; and after annealing at 2000°C with (b) 10 wt% Fe and (c) 40 wt% Fe.

With increasing Fe concentration from 10 wt% to 40 wt%, the relative molar Fe abundance varies from about 37% to 21% for paramagnetic Fe, 4% to 1% for α-Fe, 47% to 68% for Fe_3C, and 12% to 9% for the unidentified ferromagnetic phase, respectively.

Figure 4a also shows Mössbauer spectra of the Fe-C samples milled for 2 hours and annealed at 1100°C, all of which consist of one singlet and two sextets. The component with a field of about 11.5 T that was observed for samples as-milled and annealed at lower temperatures is not observed in the present spectra. Only the components with hyperfine fields of near 33.0 T and 20.0 T can be observed. Also, the relative areas of singlet and sextets are very similar for the Fe-C samples with Fe concentrations from 10 wt% to 30 wt%, while for the sample with 40 wt% Fe, the higher splitting sites are somewhat more prevalent. Similarly, as above, two ferromagnetic phases for α-Fe and Fe_3C are

Table II. Center shifts (δ), center shift (δ1, δ2), FWHM (Γ), hyperfine fields (H), quadrupole splitting (Δ), and site populations (A) for the singlet, doublet and sextet used to fit the Mössbauer spectra of the Fe-C powders with different Fe contents milled for 2 hours before and after annealing at 200°C, 1100°C, and 2000°C, respectively. Experimental uncertainties for velocities are typically ±0.005 mm/s, for hyperfine fields are ±0.1 T and for areas are ±1%.

	Singlet			Doublet							Sextet								
Sample	δ (mm/s)	Γ (mm/s)	A (%)	δ1 (mm/s)	Δ1 (mm/s)	A1 (%)	δ2 (mm/s)	Δ2 (mm/s)	A2 (%)	A (%)	H1 (T)	A1 (%)	H2 (T)	A2 (%)	H3 (T)	A3 (%)	H4 (T)	A4 (%)	A (%)
As milled, 10 wt%	-	-	-	0.369	1.450	5.1	0.277	0.962	31.2	36.3	32.9	4.1	20.3	47.9	11.6	11.7	-	-	63.7
200°C, 10 wt%	-	-	-	0.367	1.467	2.4	0.293	0.940	36.2	38.6	33.1	3.5	20.3	45.9	11.4	12.0	-	-	61.4
1100°C, 10 wt%	−0.089	0.178	12.5	-	-	-	-	-	-	-	33.0	53.1	20.2	34.4	-	-	-	-	87.5
2000°C, 10 wt%	−0.058	0.098	0.6	-	-	-	-	-	-	-	31.7	17.5	23.3	23.4	18.9	31.7	7.6	26.8	99.4
As milled, 20 wt%	-	-	-	0.369	1.469	2.4	0.266	0.953	28.2	30.6	32.9	3.6	20.3	54.8	11.5	11.0	-	-	69.4
200°C, 20 wt%	-	-	-	0.367	1.437	3.6	0.273	0.895	29.4	30.0	33.1	3.5	20.3	52.0	11.5	11.5	-	-	67.0
1100°C, 20 wt%	−0.089	0.172	13.7	-	-	-	-	-	-	-	33.0	71.5	20.5	14.8	-	-	-	-	86.3
As milled, 30 wt%	-	-	-	0.356	1.420	2.3	0.258	0.915	24.9	27.2	32.9	1.6	20.3	60.8	11.3	10.4	-	-	72.8
200°C, 30 wt%	-	-	-	0.354	1.471	2.6	0.259	0.959	23.2	25.8	32.8	1.5	20.2	59.7	11.2	13.0	-	-	74.2
1100°C, 30 wt%	−0.088	0.159	14.5	-	-	-	-	-	-	-	32.9	76.4	20.6	9.1	-	-	-	-	85.5
As milled, 40 wt%	-	-	-	0.370	1.478	1.3	0.252	0.946	20.5	21.8	33.1	1.3	20.3	67.9	11.4	9.0	-	-	78.2
200°C, 40 wt%	-	-	-	0.368	1.435	1.5	0.247	0.903	18.8	20.3	33.0	1.5	20.2	68.9	11.2	9.3	-	-	79.7
1100°C, 40 wt%	−0.088	0.169	5.5	-	-	-	-	-	-	-	33.0	86.3	20.6	8.2	-	-	-	-	94.5
2000°C, 40 wt%	−0.043	0.285	3.2	-	-	-	-	-	-	-	33.2	53.8	30.3	20.9	23.8	22.1	-	-	96.8

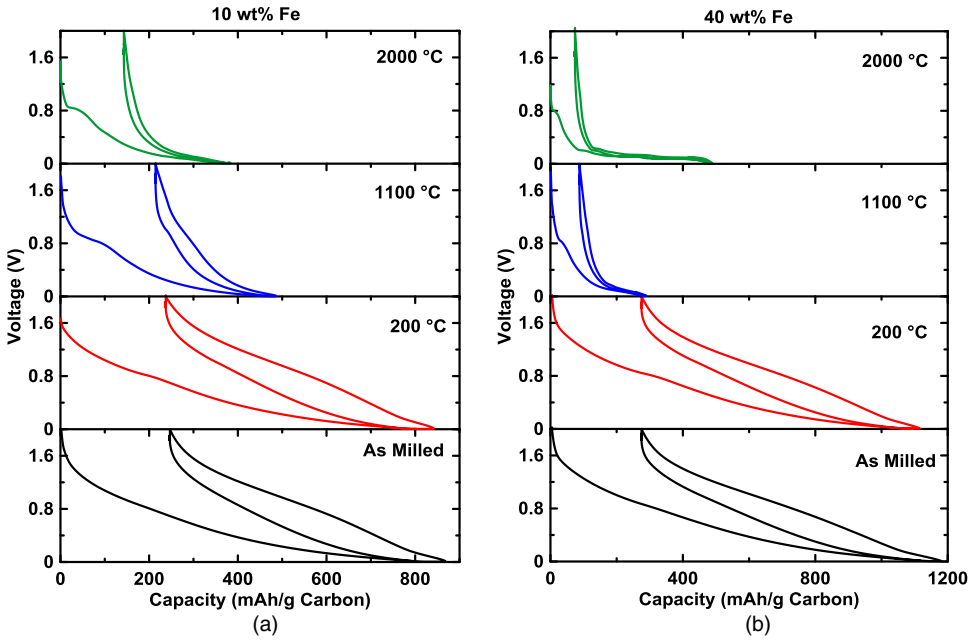

Figure 5. Voltage curves of the Fe-C samples with (a) 10 wt% Fe and (b) 40 wt% Fe.

represented by two sextets with the hyperfine magnetic fields of 33.0 T and 20.0 T, respectively. Generally, a singlet close to zero velocity (with respect to α-Fe) can be due to either γ-Fe or superparamagnetic α-Fe.[24] Preston et al.[25] and Kovats et al.[26] gave a center shift of about −0.04 mm/s for γ-Fe relative to α-Fe. Therefore the difference between alpha and gamma phase center shifts is very small. However, Mao et al. have reported that the superparamagnetic Fe precipitates observed in Fe-Sn compounds have both a more positive center shift of +0.144 mm/s and a measurable quadrupole splitting.[27] Therefore, for the samples mentioned above, a singlet with a slight negative center shift of about −0.09 mm/s and the lack of quadrupole splitting, as listed in Table II, can most likely be attributed to the γ-Fe phase.

It can be found from the results and analysis above, when the annealing temperature is raised to 1100°C, α-Fe, Fe_3C and γ-Fe phases appear in the Fe-C samples. Compared to those as-milled and annealed at 200°C samples, much more α-Fe and a reduced Fe_3C content are present in the 1100°C samples, along with the occurrence of γ-Fe phase and disappearance of the unidentified ferromagnetic phase. Moreover, the Fe concentration has a significant effect on the relative concentration of these phases in the 1100°C Fe-C samples. As listed in Table II, the relative molar Fe abundance increases from about 53% to 86% for α-Fe and decreases from 34% to 8% for Fe_3C, respectively, when the Fe concentration varies from 10 wt% to 40 wt%.

For the sample with 10 wt% Fe milled for 2 hours and annealed at 2000°C, a complex Mössbauer spectrum is observed, as shown in Figure 4b. This includes one singlet with a center shift of −0.058 mm/s and four sextets with the hyperfine fields of 31.7 T, 23.3 T, 18.9 T, and 7.6 T. The singlet corresponds to a γ-Fe phase with a relative molar Fe abundance of 0.6%. The four sextets with relative molar Fe abundances of about 18%, 23%, 32% and 27%, respectively, cannot be identified to any specific ferromagnetic phases, although they correspond to Fe sites with differing near-neighbor Fe and C coordination numbers. The 31.7 T may result from α-Fe with a small amount of C, the 23.3 T and 18.9 T phases may result from off-stoichiometric or disordered Fe_3C. The 7.6 T phase results from Fe in a very C-rich environment.

The spectrum of the sample with 40 wt% Fe after annealing at 2000°C, as shown in Figure 4c, is best fit to a combination of one singlet with a center shift of −0.044 mm/s and three sextets with the hyperfine fields of 33.2 T, 30.3 T, and 23.8 T, indicating the presence of a γ-Fe phase, as well as three different Fe sites. The site with the hyperfine field of 33.2 T can be assigned to α-Fe phase, which is present with relative molar Fe abundance of about 54%. The other two sites with the relative molar Fe abundances of 21% and 22% respectively cannot be identified with any specific phases, although they may be similar to two of the phases discussed for the 10 wt% sample above.

Electrochemical characterization.—Figure 5a shows the voltage curves of the as milled and annealed 10 wt% Fe samples in Li cells. To our knowledge both the iron and Fe_3C phases are inactive to lithium.[8] Therefore, in order to compare the effect of Fe content and heat-treatment on the electrochemical performance of the carbon phase more meaningfully, the capacities of Fe-C samples were calculated based on the carbon mass. The data plotted are for the first 1.5 half-cycles and the reversible capacity of these cells are plotted in Figure 1, in order to compare to previous studies. The voltage profiles of the as-milled and 200°C annealed 10 wt% Fe-C electrodes have high capacity and a large hysteresis between charge and discharge cycles and have reversible capacities of about 600 mAh/g, which are typical of ball-milled carbons, as shown in Figure 1.

The voltage curve of the 1100°C annealed 10 wt% Fe-C sample has a significantly reduced reversible capacity and lower hysteresis than the lower temperature samples. It has been suggested previously that the reversible capacity of the ball milled carbon is partly derived from the presence of free radical carbons.[17] If this is the case, then annealing ball milled carbons ought to reduce the free radical carbon content and result in a reduced reversible capacity, as observed here. The resulting carbon has a voltage curve and reversible capacity typical of turbostratically disordered graphites made at this temperature, which have blocked channels for intercalation, as shown in Figure 1. The voltage curve of the 2000°C annealed 10 wt% Fe-C sample has still lower hysteresis and is typical of turbostratically disordered hard or soft carbons heated to this temperature.

Figure 5b shows the voltage curves of the 40 wt% Fe samples milled for 2 hours. The reversible capacities of these cells are also plotted in Figure 1 for comparison to previous studies. Compared to those samples with 10 wt% Fe, the voltage curves of the as-milled and 200°C annealed samples are very similar, however their reversible capacities are significantly higher, as shown in Figure 1. This agrees with a growing body of evidence that the presence of inactive transition metals can significantly increase the capacity of

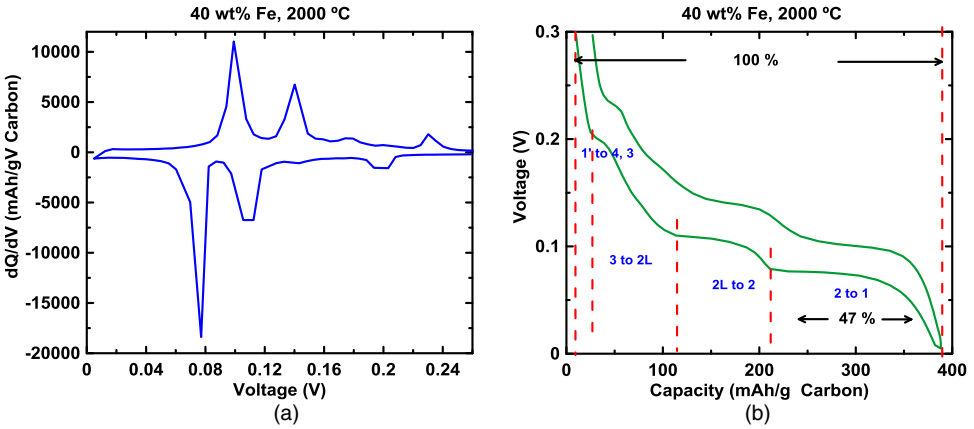

Figure 6. The second cycle (a) differential capacity and (b) voltage curve of Fe-C powder after annealing at 2000°C with 40 wt% Fe.

carbon.[8–10,15] For 40 wt% Fe samples annealed at 1100°C, the capacity is greatly reduced and voltage curve is similar to a disordered graphite electrode. Compared to the 10 wt% Fe sample, the 40 wt% Fe sample at 1100°C has greatly reduced hysteresis and irreversible capacity, indicating that the Fe has some catalytic effect on the structure of the graphite.

When the annealing temperature is increased to 2000°C, the 40 wt% Fe sample shows an electrochemical behavior that is identical to a graphite electrode. This graphitic character can be easily seen in the well-defined peaks in differential capacity curve of this electrode, shown in Figure 6a. To the best of our knowledge, this is the first report of ball-milled carbon that has been fully graphitized at a relatively low temperature of 2000°C. As well, the reversible capacity is increased significantly from about 197 mAh/g to 407 mAh/g when the annealing temperature of the 40 wt% Fe samples is increased from 1100°C to 2000°C. In fact, the reversible capacity for the 2000°C sample is higher than that of the theoretical capacity of graphite. This anomalously high capacity is likely be due to an underestimation of the active carbon in the electrode, since some Fe was found to have been ejected from the sample in the fluctuating magnetic field of the induction furnace. Indeed, by TGA measurements we have found that this sample consisted of only 17 wt% Fe, according to the sample forming CO_2 and Fe_2O_3 when heated in air. The exact amount of active carbon cannot be determined by this method, however, as the Mössbauer results have shown that this sample comprises both Fe and Fe-carbides of unknown stoichiometry.

An estimate of the true capacity of the 40 wt% Fe-C 2000°C sample can be obtained by analysis of its voltage curve, since the length of the stage 2 - stage 1 plateau is a good measure of the extent of graphitization. This plateau is 50% of the total capacity for fully graphitized carbon and monotonically decreases as the fraction of the total capacity with increased turbostratic disorder.[28] The voltage curve in the second cycle of the 40 wt% Fe-C 2000°C sample is plotted in Figure 6b. The stage 2 - stage 1 plateau is about 47% of the total graphite capacity. This value is consistent with that of highly ordered commercial graphites (e.g. in Ref. 22) that have capacities near 370 mAh/g and is also consistent with the high level of graphitization measured above by XRD diffraction. Thus, considering all the plateaus of pristine graphite are observed in the voltage curve of the 40 wt% Fe-C 2000°C sample, LiC_6 is clearly formed at full lithiation. Therefore we believe the capacity of this graphite sample is likely near 370 mAh/(g carbon), which is the value plotted in Figure 1. This is much higher than expected for a hard or soft carbons heated at this temperature with no catalysts, as shown in Figure 1. The electrochemical performance of all the Fe-C samples are listed in Table III.

Figure 7a shows the cycling performance of the 10 wt% Fe samples. The as-milled sample and the sample after annealing at 200°C have reversible capacities of about 480 mAh/g based on the carbon mass and show some fade. The Fe-C samples annealed at 1100°C and 2000°C, both show good cycling performance with specific capacities of about 220 mAh/g based on the carbon mass after 30 cycles. The cycling performance of the Fe-C samples with 40 wt% Fe content is shown in Figure 7b. The as-milled and 200°C samples have high capacities, but show some capacity fade. By comparison, the 1100°C sample has much better cycling performance, but low reversible capacity. The 40 wt% Fe sample that was graphitized by annealing at 2000°C has excellent cycling performance and low capacity loss, and characteristic of well graphitized carbon.

Figure 8 shows the SEM image of the 40 wt% Fe sample. It comprises small Fe particles that are dispersed amongst graphite particles that are about 20 μm in size. This sample has a density of 2.34 g/cm^3, as determined by He gas pycnometery. The gravimetric capacity based on the whole Fe-C composite mass is 244 mAh/g. Graphite is known to expand 10% by volume during full lithiation, so the volume expansion of Fe-C composite is estimated between 5% and 10% based on the 17 wt% Fe in the sample measured by TGA. Based on the results above, the estimated volumetric capacity is between 544 Ah/L and 520 Ah/L. It is lower than that of commercial graphite (720 Ah/L). This can be partly due to the low density of this powder and existence of inactive iron carbides. Appropriate carbon sources should be investigated to increase density in the future. Nevertheless, to our knowledge this is the first report of the electrochemical performance of catalytically formed graphite in Li cells. The good characteristics of the catalytically derived graphites found here shows that this may be a fruitful area for research in high performance Li-ion graphites.

Table III. Summary of the electrochemical performance of the Fe-C samples in Li cells. DC = 1st specific discharge capacity; RC = 1st specific charge capacity; IRC = irreversible capacity; ICE = initial coulombic efficiency, and Cycle 30 = the 30th specific charge capacity. All capacities are calculated based on the carbon mass. The uncertainty for capacities is typically ±1 mAh/g.

Sample	DC (mAh/g)	RC (mAh/g)	IRC (mAh/g)	ICE (%)	Cycle 30 (mAh/g)
As milled, 10 wt%	868	621	247	72	487
200°C , 10 wt%	842	604	237	72	472
1100°C, 10 wt%	486	271	214	56	222
2000°C, 10 wt%	375	232	143	62	219
As milled, 40 wt%	1181	906	275	77	742
200°C , 40 wt%	1116	841	275	75	683
1100°C, 40 wt%	284	197	88	69	183
2000°C, 40 wt%*	437	370	67	85	360

*Capacities for this sample are estimated from analysis of voltage curve, as explained in the text.

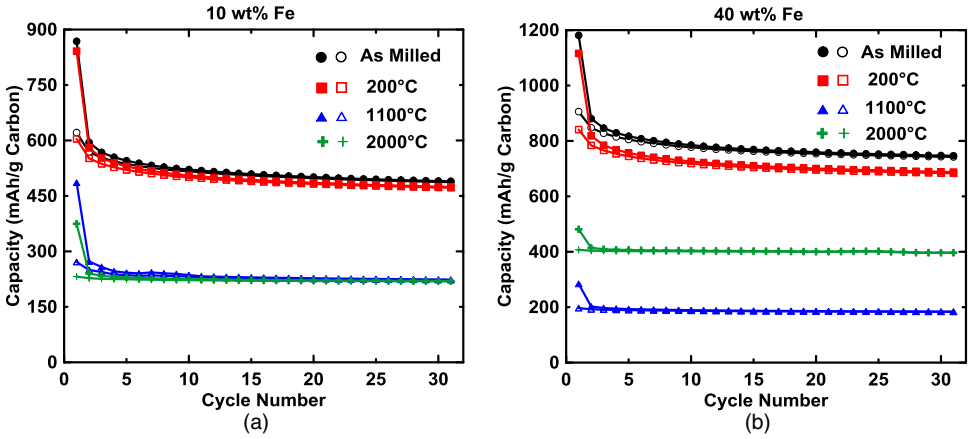

Figure 7. Cycling performance of the Fe-C samples with (a) 10 wt% Fe and (b) 40 wt% Fe.

Conclusions

Fe-C composites with 10 - 40 wt% Fe (2.3 - 12.5 atomic %) were made by ball milling and subsequently annealing at temperatures up to 2000°C. When the samples were annealed at temperatures above 1100°C, the increased Fe content favors the crystallization of carbon via a catalytic graphitization process. Full graphitization resulted when the Fe content was 40 wt% and an annealing temperature of 2000°C was used. Mössbauer effect studies indicated that Fe concentration, annealing time, and annealing temperature, have significant effects on the magnetic splitting, quadrupole splitting, and the formation of the γ-Fe phase of Fe-C powders. Typically, the relative concentration of the ferromagnetic phase increases while the relative concentration of the paramagnetic phase decreases with increasing of Fe content for the Fe-C samples in which the spectra consist of both sextets and doublets. Moreover, annealing at a temperature of 200°C has no obvious effect on the microstructure of Fe-C powders, but high temperature annealing at 1100°C or 2000°C typically results in the formation of the γ-Fe phase in the ball-milled samples.

The electrochemistry of Fe-C electrodes was strongly dependent on the crystalline structure of the carbon phase, which is associated with the Fe concentration and annealing temperature. Fe-C samples with amorphous carbons (i.e. as-milled and samples annealed at 200°C) showed higher initial irreversible capacity, higher reversible capacity, and larger hysteresis than those which have been shown to contain a significant graphitic component (i.e. samples annealed at 1100°C or 2000°C). Ball-milled Fe-C with 40 wt% Fe in the starting materials and annealed at 2000°C showed characteristics of a well ordered graphite electrode, with clear evidence of staging and excellent cycling characteristics.

This is the first report that we know of that describes the catalytic full graphitization of a ball-milled carbon. It has been shown here that such graphites can have good performance in electrochemical cells. Typically synthetic graphites are made at much higher temperatures (∼3000°C). The use of graphites that have been catalytically formed at lower temperatures may provide substantial cost savings and allow more avenues for the design of graphite materials for lithium batteries. Further work is needed to explore this synthesis route for graphite anodes. In particular, different carbon sources, catalysts and methods of removing the catalyst after graphitization should be explored.

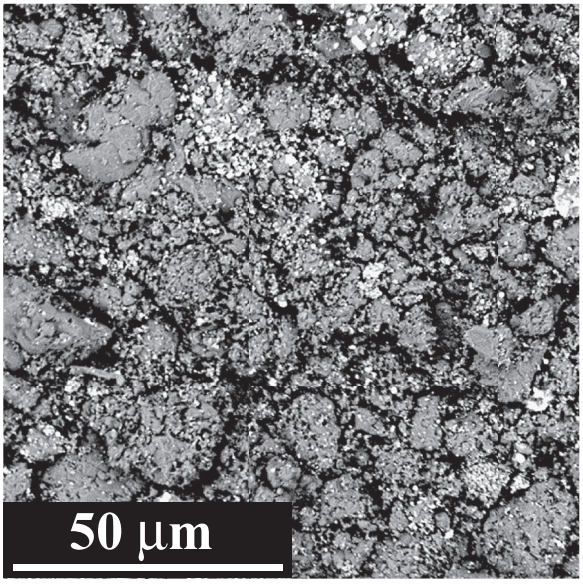

Figure 8. SEM image of the Fe-C sample milled for 2 h and annealed at 2000°C with 40 wt% Fe.

Acknowledgments

The authors acknowledge funding from NSERC and 3M Canada, Co. under the auspices of the Industrial Research Chair and Discovery grant programs and for financial support from the Dalhousie Research in Energy Advanced Materials and Sustainability (DREAMS) program. The authors thank Professor J. R. Dahn for assistance with the CARBONXS software.

References

1. J. R. Dahn, Tao Zheng, Yinghu Liu, and J. S. Xue, *Science*, **270**, 590 (1995).
2. Z. Ogumi and H. Wang, *Lithium-Ion Batteries Science, Technologies*, M. Yoshio, R. J. Brodd, and A. Kozawa editors, Springer (2009).
3. M. Yoshio, H. Wang, K. T. Umeno, T. Abe, and Z. Ogumi, *J. Mater. Chem.*, **14**, 1754 (2004).
4. A. Oya and H. Marsh, *J. Mater. Sci.*, **17**, 309 (1982).
5. S. Otani Oya, *Carbon*, **17**, 131 (1979).
6. C. Baraniecki, P. H. Pinchbeck, and F. B. Pickering, *Carbon*, **7**, 213 (1969).
7. M. N. Obrovac, X. Y. Zhao, L. T. Burke, and R. A. Dunlap, *Electrochem. Commu.*, **60**, 221 (2015).
8. X. Y. Zhao, D. G. Xia, J. C. Yue, and S. Z. Liu, *Electrochim. Acta*, **116**, 292 (2014).
9. J. C. Yue, X. Y. Zhao, and D. G. Xia, *Electrochem. Commu.*, **18**, 44 (2012).
10. J. M. Skowronski and K. Knofczynski, *J. Power Sources*, **194**, 81 (2009).
11. J. M. Skowronski and K. Knofczynski, *J. New Mat. Electrochem. Systems*, **9**, 359 (2006).
12. T. Tanaka, S. Nasu, K. N. Ishihara, and P. H. Shingu, *J Less-Commom Metals*, **171**, 237 (1991).
13. G. M. Wang, S. J. Campbell, A. Calka, and W. A. Kaczmarek, *Nanostruct. Mater.*, **6**, 389 (1995).
14. M. A. Al-Maghrabi, R. J. Sanderson, and R. A. Dunlap, *Philos. Mag.*, **93**, 3278 (2013).
15. X. Y. Zhao, R. J. Sanderson, L. MacEachern, R. A. Dunlap, and M. N. Obrovac, *Electrochim. Acta.*, **170**, 16 (2015).

16. F. Disma, L. Aymard, L. DuPont, and J. M. Tarascon, *J. Electrochem. Soc.*, **143**, 3959 (1996).
17. W. Xing, R. A. Dunlap, and J. R. Dahn, *J. Electrochem. Soc.*, **145**, 62 (1998).
18. J. R. Dahn, A. K. Sleigh, H. Shi, J. N. Reimers, Q. Zhong, and B. M. Way, *Electrochim. Acta*, **38**, 1179 (1993).
19. K. Lagarec and D. G. Rancourt, Recoil: Mössbauer spectral analysis software for windows, http://www.isapps.ca/recoil/ (1998).
20. International Centre for Diffraction Data PDF-2 and Release .
21. H. Shi, J. N. Reimers, and J. R. Dahn, *J. Appl. Cryst.*, **26**, 827 (1993).
22. T. Zheng, J. N. Reimers, and J. R. Dahn, *Phys. Rev. B*, **51**, 734 (1995).
23. G. Le Caër and P. Matteazzi, *Hyperfine Interact.*, **66**, 309 (1991).
24. G. Longworth and R Jain, *J. Phys. F: Met. Phys.*, **8**, 993 (1978).
25. R. S. Preston, S. S. Hanna, and J. Heberle, *Phys. Rev.*, **128**, 2207 (1962).
26. T. A. Kovats and J. C. Walker, *Phys. Rev.*, **181**, 610 (1969).
27. O. Mao, R. A. Dunlap, and J. R. Dahn, *J. Electrochem. Soc.*, **146** , 405 (1999).
28. T. Zheng and J. R. Dahn, *Phys. Rev. B*, **53**, 3061 (1996).